EJN fens EUROPEAN JOURNAL OF NEUROSCIENCE

European Journal of Neuroscience, Vol. 33, pp. 843–855, 2011 doi:10.1111/j.1460-9568.2010.07578.x

MOLECULAR AND DEVELOPMENTAL NEUROSCIENCE

Involvement of endoplasmic reticulum stress on neuronal cell death in the lateral geniculate nucleus in the monkey glaucoma model

Yasushi Ito,[1] Masamitsu Shimazawa,[1,2] Yuta Inokuchi,[1] Hajime Yamanaka,[2] Kazuhiro Tsuruma,[1] Kazuyuki Imamura,[3] Hirotaka Onoe,[2] Yasuyoshi Watanabe,[2] Makoto Aihara,[4] Makoto Araie[4] and Hideaki Hara[1,2]

[1]Molecular Pharmacology, Department of Biofunctional Evaluation, Gifu Pharmaceutical University, 1-25-4 Daigaku-Nishi, Gifu 501-1196, Japan

[2]RIKEN Center for Molecular Imaging Science, Kobe, Hyogo, Japan

[3]Department of Systems Life Engineering, Maebashi Institute of Technology, Maebashi, Gunma, Japan

[4]Department of Ophthalmology, University of Tokyo School of Medicine, Tokyo, Japan

Keywords: apoptosis, cynomolgus monkey, immunohistochemistry, ocular hypertension

Abstract

We investigated whether endoplasmic reticulum (ER) stress was involved in the pathophysiological mechanisms underlying neuronal death of the lateral geniculate nucleus (LGN) after intraocular pressure (IOP) elevation. Five cynomolgus monkeys, four with a glaucomatous left eye after laser photocoagulation treatment and one normal monkey, were studied. At 4, 11, 15 and 24 weeks after the laser photocoagulation treatment, the numbers of LGN neurons and atrophy were immunohistochemically evaluated using anti-parvalbumin-antibody, which was used to specifically label relay neurons connecting to the visual cortex. In addition, terminal deoxynucleotidyl transferase-mediated dUTP nick end labeling (TUNEL)-positive cells, polyubiquitin, and production of ER stress-related proteins, such as the phosphorylation of eukaryotic initiation factor 2α (p-eIF2α) and C/EBP-homologous protein (CHOP), were also measured using *in situ* hybridization and immunostaining. Loss of neurons and/or neuronal atrophy in layers 1, 4 and 6 of the LGN on the contralateral side were observed at 4–24 weeks after the laser photocoagulation treatment. Furthermore, the retinal input from the high IOP eye projected to layers 2 (magnocellular layer), 3 and 5 (parvocellular layer) on the ipsilateral side. Neuronal damage was also confirmed in these layers. In the LGN region, TUNEL-positive cells, polyubiquitin, p-eIF2α and CHOP were also detected at 11–24 weeks after the laser photocoagulation treatment. These findings indicate that ER stress may play a pivotal role in neuronal death of the LGN after IOP elevation.

Introduction

Glaucoma, an optic neuropathy resulting from retinal ganglion cell (RGC) death, is one of the leading causes of blindness worldwide (Resnikoff *et al.*, 2004). Recent evidence indicates that glaucomatous damage extends from the retina to the visual center of the brain, including the lateral geniculate nucleus (LGN) and the primary visual cortex (Gupta & Yücel, 2003; Vrabec & Levin, 2007; Yücel & Gupta, 2008). In particular, neuronal damage in the LGN in monkey glaucoma models can be detected in the early phase (the first few weeks) after intraocular pressure (IOP) elevation (Weber *et al.*, 2000; Ito *et al.*, 2009a). Furthermore, relay neurons, a type of LGN neuron that proceed to synapse in the visual cortex, were more vulnerable than the other types of LGN neurons after IOP elevation (Jones & Hendry, 1988; Johnson & Casagrande, 1995). In addition, most of the degenerative and compensatory changes in the LGN occur in the relay neurons after total deafferentation (Le Vay, 1971; Somogyi *et al.*, 1987). Therefore, protecting relay and retinal neurons may be effective in preventing blindness in glaucoma cases because visual information entering the eye is processed in the retina and then transmitted to the LGN, from where signals are relayed to the visual cortex.

Recently, we found that endoplasmic reticulum (ER) stress may play a pivotal role in RGC death induced by IOP elevation in mice (Shimazawa *et al.*, 2007a). ER stress is caused by the accumulation of misfolded or unfolded proteins within the ER lumen. The excess ER stress leads to ER stress-induced cell death, highlighting the possible mechanisms of neurodegenerative diseases, such as Alzheimer's disease, amyotrophic lateral sclerosis and Parkinson's disease (Aridor & Balch, 1999; Kaufman, 1999; Harding *et al.*, 2002; Nakamura & Lipton, 2009). In fact, the accumulation of polyubiquitinated proteins and increased ER stress-related proteins [e.g. C/EBP homologous protein (CHOP, also known as GADD153) and the phosphorylation of eukaryotic initiation factor 2α (p-eIF2α)] were observed in these diseases (Oyadomari & Mori, 2004; Ilieva *et al.*, 2007; Ito *et al.*, 2009b). However, the involvement of ER stress-induced cell death in

Correspondence: Dr H. Hara, [1]Molecular Pharmacology, as above.
E-mail: hidehara@gifu-pu.ac.jp

Received 2 July 2010, revised 29 November 2010, accepted 1 December 2010

© 2011 The Authors. European Journal of Neuroscience © 2011 Federation of European Neuroscience Societies and Blackwell Publishing Ltd

LGN neurons after IOP elevation has not been reported. Therefore, we investigated whether ER stress-related proteins, especially p-eIF2α and CHOP, are involved in neuronal death after IOP elevation in the LGN of monkeys.

Methods

Animals

Five adult male cynomolgus monkeys (*Macaca fascicularis*) aged 4–6 years (Nippon SLC, Hamamatsu, Japan) were used – four with a glaucomatous left eye after laser photocoagulation treatment and one normal monkey. Each monkey was housed in an individual cage within a monkey colony. Ophthalmoscopic examinations conducted before the experiment revealed no ocular abnormalities in any of the monkeys. All experiments were performed in accordance with the Association for Research in Vision and Ophthalmology Statement for the Use of Animals in Ophthalmic and Vision Research and were approved and monitored by the Institutional Animal Care and Use Committee of RIKEN Center for Molecular Imaging Science.

Induction of experimental glaucoma

Elevated IOP was induced by applying argon blue/green laser photocoagulation burns (Ultima 2000 SEl; Coherent Inc., Santa Clara, CA, USA) to the trabecular meshwork of the left eye. The right eye was used as an untreated control, as previously described (Quigley & Hohman, 1983).

Histological analysis of RGC axons

After the final IOP measurement at 4–24 weeks after the first laser treatment, the monkeys were perfused via the common carotid artery with 0.9% saline containing 10 U/mL heparin at room temperature, followed by 4% paraformaldehyde in 0.01 M phosphate-buffered saline (PBS; pH 7.4). This was done under deep general anesthesia (sodium pentobarbital). Eyeballs were enucleated and 4% paraformaldehyde in PBS solution was injected into the vitreous body and postfixed by immersion in 4% paraformaldehyde in PBS for at least 24 h at 4 °C. After eyeballs had been enucleated, a 3-mm-long segment of the optic nerve was cut out at 6–9 mm distance from the eyeball–optic nerve junction, and was postfixed by immersion in 4% paraformaldehyde in PBS for at least 24 h at 4 °C. The eyeballs and optic nerve segments were soaked in 10, 15 and 30% (w/v) sucrose in 0.1 M phosphate buffer, pH 7.4, at 4 °C for at least 24 h each, and then frozen in embedding compound. Frozen sections (thickness, 20 μm) cut through the optic disc of each eye were prepared in a standard manner, and stained with hematoxylin and eosin. Coronal sections of the optic nerve segment were cut at 10-μm thickness and every 20th section was mounted onto the same slide glass (MAS-COAT; Matsunami, Osaka, Japan) until we obtained 20 slide glasses each mounting four sections. As cutting of sections was started from the end closer to the eyeball, the sections to be evaluated for counting should be 6–7 mm distant from the eyeball–nerve junction. Sections were washed with 0.01 M PBS, preincubated with 10% normal goat serum in 0.01 M PBS for 30 min, and then incubated overnight at 4 °C with mouse anti-phosphorylated neurofilament H (SMI-31) monoclonal antibody (1 : 1000 dilution) (NE1022; Calbiochem, San Diego, CA, USA). They were washed with 0.01 M PBS and then incubated for 3 h at room temperature with a mixture of Alexa Fluor 546 $F(ab')_2$ fragment of goat anti-mouse IgG (H+L) (1 : 1000 dilution) (A-11018; Molecular Probes, Portland, OR, USA). For counting of the numbers of SMI-31-positive RGC axons, we randomly chose a single slide glass from 20, and identified five regions (nasal, temporal, superior, inferior and central) in each of four optic nerve sections. In each center of the regions, we placed a sample volume of interest with a size of 218 × 164 × 10 (section thickness) μm under a microscope fitted with × 40 objective and × 3 digital zoom; thus, 0.18 mm^2 per section was assessed for counting the numbers of SMI-31-positive RGC axons. The counting, as well as photographing, was performed by a single observer (Y.I.). Thereby, for each optic nerve, we obtained 20 measurements of axon density (five regions × four sections).

Histological analysis of LGN

Brains were removed at the time of eyeball removal after the perfusion. Brains were cut into several sections and immersed in the same fixative solution for at least 24 h, soaked in 10–30% (w/v) sucrose, then frozen in embedding compound (Tissue-Tek; Sakura Finetechnical Co. Ltd, Tokyo, Japan). Next, 20-μm-thick coronal sections of the LGN were serially cut.

To detect apoptotic cells, a terminal deoxynucleotidyl transferase-mediated dUTP nick end labeling staining (TUNEL) assay was performed according to the manufacturer's instructions (Roche Molecular Biochemicals Inc., Mannheim, Germany).

During the immunofluorescent staining procedures, coronal sections containing LGN were subjected to antigen retrieval by autoclaving in 0.01 M sodium citrate buffer, pH 6.0, at 121 °C for 15 min, then treated with 0.3% hydrogen peroxidase in 0.01 M PBS. They were then preincubated with 10% normal goat serum (Vector Laboratories Inc., Burlingame, CA, USA) in 0.01 M PBS for 30 min, then incubated for 1 day at 4 °C with specific mouse anti-parvalbumin monoclonal antibody (1 : 1000 dilution) (MAB 1572; Chemicon, Temecula, CA, USA), mouse anti-polyubiquitin monoclonal antibody (1 : 1000 dilution) (FK2; Nippon Biotest Laboratories Inc., Tokyo, Japan), rabbit anti-p-eIF2α polyclonal antibody (1 : 100 dilution, Ser 51; Cell Signaling Technology, Danvers, MA, USA) and rabbit anti-CHOP polyclonal antibody (1 : 1000 dilution, F-168; Santa Cruz Biotechnology, Santa Cruz, CA, USA) in a solution of 10% normal goat serum in 0.01 M PBS containing 0.3% (v/v) Triton X-100. The coronal sections were then washed with PBS and incubated with biotinylated anti-mouse or anti-rabbit IgG before being incubated with avidin–biotin–peroxidase complex for 30 min at room temperature. Finally, diaminobenzidine was used as a peroxidase substrate for visualization.

To visualize co-localization of CHOP with parvalbumin, double immunofluorescence was performed on LGN sections. Coronal sections containing LGN were washed with 0.01 M PBS. Next, they were preincubated with 10% normal goat serum in 0.01 M PBS for 30 min, then incubated overnight at 4 °C with mouse anti-parvalbumin monoclonal antibody (1 : 1000 dilution) and rabbit anti-CHOP polyclonal antibody (1 : 1000 dilution) in a solution of 10% normal goat serum in 0.01 M PBS with 0.3% (v/v) Triton X-100. Next, they were washed with 0.01 M PBS and then incubated for 3 h at room temperature with a mixture of an Alexa Fluor 488 $F(ab')_2$ fragment of goat anti-rabbit IgG (H+L) (1 : 1000 dilution, A11070; Molecular Probes) and an Alexa Fluor 546 $F(ab')_2$ fragment of goat anti-mouse IgG (H+L) (1 : 1000 dilution, A-11018; Molecular Probes). At the end of immunostaining, Hoechst 33342 (1 : 5000 dilution) was added to the samples for 30 min to visualize the nuclei.

For quantification of parvalbumin-immunostained sections, every third section was mounted onto a glass slide and immunostained.

© 2011 The Authors. European Journal of Neuroscience © 2011 Federation of European Neuroscience Societies and Blackwell Publishing Ltd

Parvalbumin-immunoreactive neurons in each layer of the LGN were estimated by counting (under a microscope fitted with a × 40 objective and × 3 digital zoom). The effects of elevated IOP on parvalbumin-immunoreactive neuronal cell size were evaluated as previously described (Ito *et al.*, 2009a), and neuron samples (100 neurons per layer) were taken randomly from the full width of each lamina and the soma area was measured. Average neuronal cell size for each layer was calculated based on data from 100 neurons.

For quantification of TUNEL-, polyubiquitin-, p-eIF2α- and CHOP-positive cells, every third section was mounted onto a glass slide. These cells were estimated by counting all clearly displayed neurons located in each layer. Three sections representative of the anterior, middle and posterior parts of each LGN were measured (Yücel *et al.*, 2000, 2001).

Statistical analysis

Soma size and number of cells are presented as mean ± SEM. Differences in mean cell number and soma size were compared using two-way ANOVA to assess the effects of side, time and side × time interaction, followed by Bonferroni's *post hoc* analysis (SPSS version 16.0; SPSS Japan, Tokyo, Japan). A value of $P < 0.05$ was considered statistically significant. Paired comparisons of LGN soma size distributions were made using the Kolmogorov–Smirnov test for two independent samples (Stat View version 5.0; SAS Institute, Inc., Cary, NC, USA).

Results

Changes in IOP, retina and optic nerve in experimental glaucoma

The IOP data are summarized in Table 1. The IOP of the monkeys was elevated and remained above baseline throughout the observation period (4–24 weeks) after the first laser photocoagulation treatment.

Although the normal right eyes from monkeys did not display morphological changes in retina, the glaucomatous left eyes exhibited time-dependent changes (decreased cell number of ganglion cell layer and inner plexiform layer thickness) after the IOP elevation (Fig. 1A).

In cross-section, the optic nerve remained roughly circular, and both its area and the number of SMI-31-positive RGC axons exhibited time-dependent decreases after IOP elevation. The cross-sectional area of the glaucomatous (left) optic nerve was decreased to 102.4, 65.1, 69.3 and 42.0% of that of the control (right) optic nerve at 4, 11, 15 and 24 weeks, respectively, after IOP elevation (Fig. 1B and C). The number of SMI-31-positive RGC axons in the glaucomatous (left) optic nerve was decreased to 47.6, 23.1, 22.6, and 19.2% of that of the control (right) optic nerve at 4, 11, 15 and 24 weeks, respectively, after IOP elevation (Fig. 1B and C, and Table 2).

TABLE 1. Changes in intraocular pressure (IOP) after laser photocoagulation treatment in cynomolgus monkeys

Animal no.	Duration (weeks)	Mean IOP (mmHg)		Left – right (ΔmmHg)	AUC
		Left	Right		
1	Normal	29.9	25.9	4.0	–
2	4	48.7	26.2	22.5	68.0
3	11	60.2	23.2	37.0	357.2
4	15	62.1	26.8	35.3	466.9
5	24	49.0	25.5	23.5	635.8

IOP was measured in both eyes in each animal using a calibrated applanation pneumatonometer (Pneumatonograph™; Alcon Inc., Fort Worth, TX, USA). The IOP of the treated monkeys was elevated and remained above baseline throughout the observation period (4–24 weeks) after the laser photocoagulation treatment. The area under the curve (AUC) is the difference in IOP between experimental glaucomatous (left) and control (right) eyes once the IOP became elevated times the number of weeks until death. IOP, intraocular pressure.

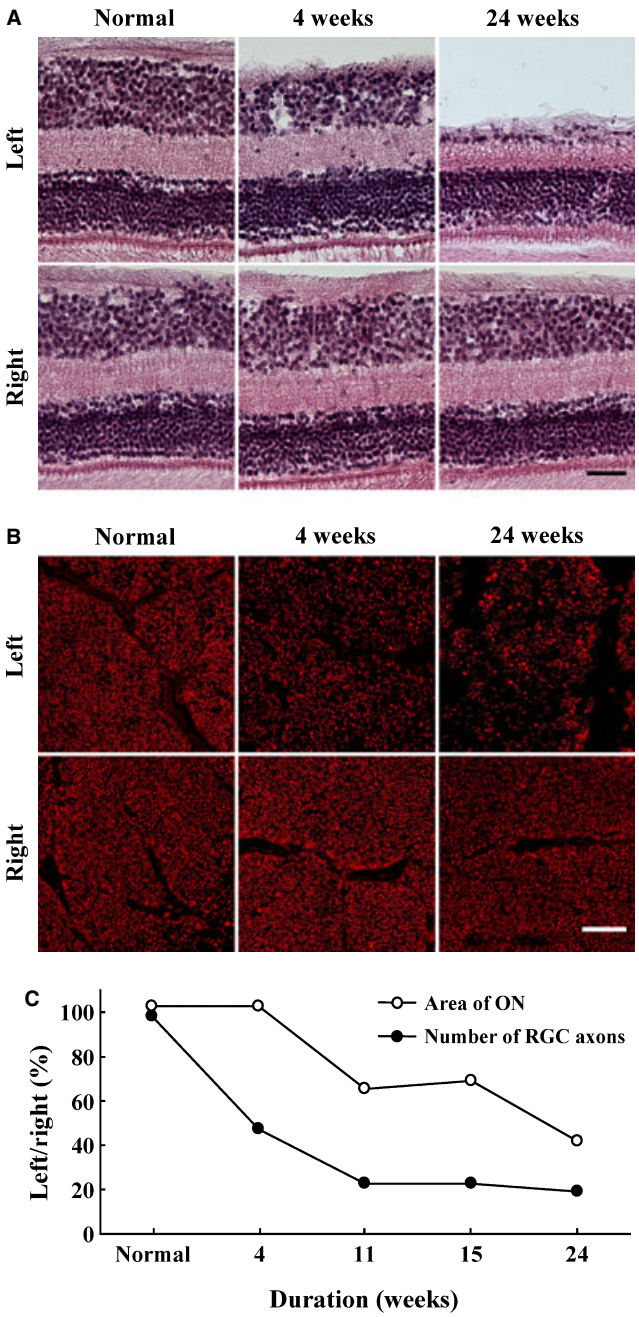

FIG. 1. (A) Representative micrographs showing hematoxylin and eosin-stained sections of retina obtained from the normal monkey and monkeys that had the pressure in their left eye elevated for 4 and 24 weeks. Scale bar = 50 μm. (B) Representative micrographs showing SMI-31-stained coronal sections of optic nerve from the normal monkey and monkeys that had the pressure in their left eye elevated for 4 and 24 weeks. Scale bar = 60 μm. (C) Cross-sectional area of optic nerve and the numbers of SMI-31-positive RGC axons. Both cross-sectional area and the RGC axon number in the glaucomatous (left) optic nerve exhibited time-dependent decreases after IOP elevation.

© 2011 The Authors. European Journal of Neuroscience © 2011 Federation of European Neuroscience Societies and Blackwell Publishing Ltd

TABLE 2. Relationship between RGC axon changes and neuronal cell death in the LGN after laser photocoagulation treatment in cynomolgus monkeys

			LGN neurons					
			Contra/Ipsi (%)			Ipsi/Contra (%)		
Animal no.	Duration (weeks)	RGC axons (left/right, %)	Layer 1	Layer 4	Layer 6	Layer 2	Layer 3	Layer 5
1	Normal	98.5	95.3	98.0	98.2	101.3	99.5	98.8
2	4	47.6	79.4	103.1	98.6	80.2	97.3	98.5
3	11	23.1	63.6	74.3	89.3	66.1	78.2	82.1
4	15	22.6	63.9	72.8	70.9	61.9	72.5	77.0
5	24	19.2	35.8	66.5	72.2	66.7	76.3	81.8

RGC axon number of the glaucomatous (left) optic nerve was decreased compared with that of the control (right) optic nerve at 4, 11, 15 and 24 weeks, after IOP elevation. The retinal input from the high IOP eye projects to layers 1, 4 and 6 on the contralateral side, and layers 2, 3 and 5 on the ipsilateral side. The numbers of neurons in layers 1, 4 and 6 of the contralateral LGN were decreased compared with those of the ipsilateral LGN at 4, 11, 15 and 24 weeks after IOP elevation. Additionally, the numbers of neurons in layers 2, 3 and 5 of the ipsilateral LGN were decreased compared with those of the contralateral LGN at 4, 11, 15 and 24 weeks after IOP elevation.

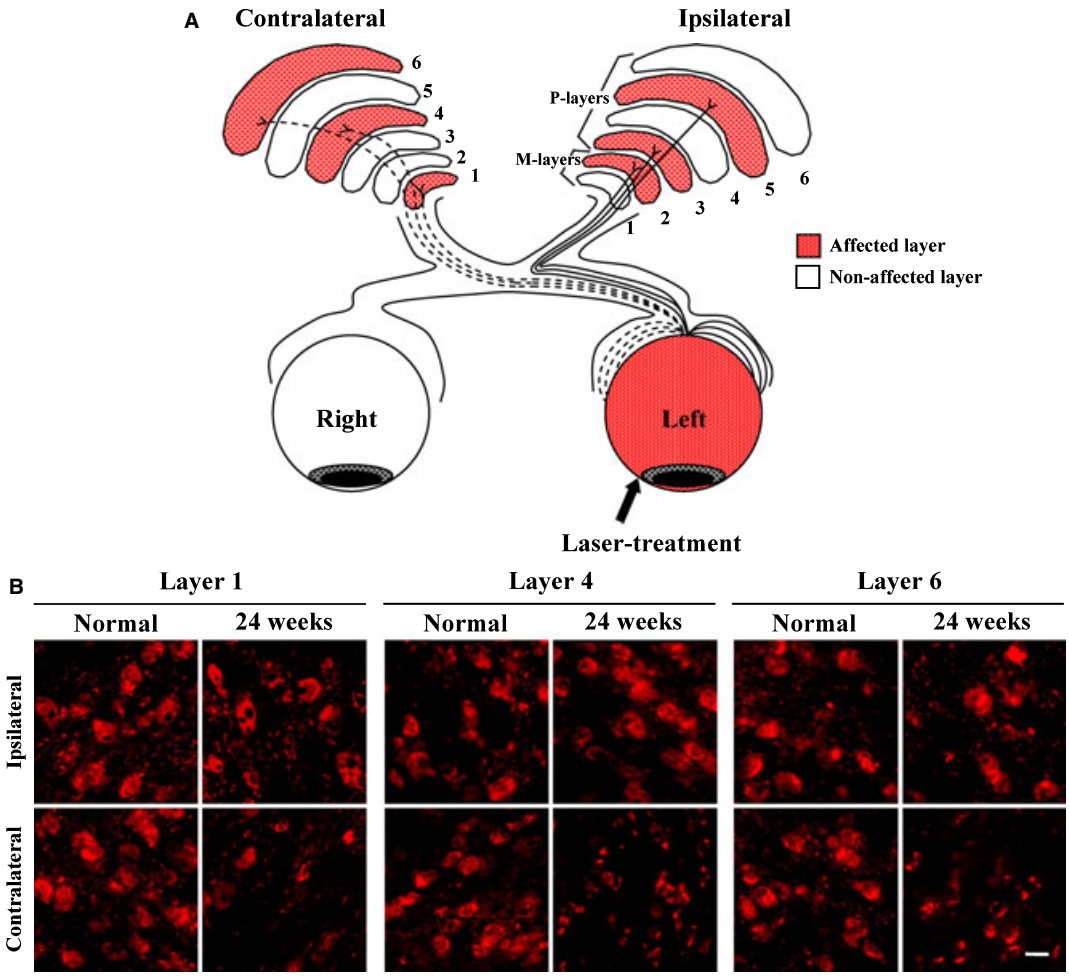

FIG. 2. (A) Layers 1, 4 and 6 on the contralateral side receive their innervations from the glaucomatous (left) eye, whereas layers 1, 4 and 6 on the ipsilateral side receive their retinal inputs from the non-treated control (right) eye. Layers 2, 3 and 5 on the ipsilateral side receive their innervations from the glaucomatous (left) eye, whereas layers 2, 3 and 5 on the contralateral side receive their retinal inputs from the non-treated control (right) eye. (B) Representative micrographs of parvalbumin-immunostained coronal sections of LGN on the contralateral and ipsilateral sides for the normal monkey and the monkey at 24 weeks after the unilateral laser photocoagulation treatment. Scale bar = 20 μm.

Neuronal damage within the LGN in experimental glaucoma

The neurons in the LGN displayed patterns of changes that differed between the contralateral (right) and ipsilateral (left) sides. Retinal input from the high IOP eye projected to layers 1 (magnocellular layer), 4 and 6 (parvocellular layer) on the contralateral side, and as predicted, neuronal losses were observed in these layers (Fig. 2A). On the ipsilateral side, the retinal input from the high IOP eye projected to

© 2011 The Authors. European Journal of Neuroscience © 2011 Federation of European Neuroscience Societies and Blackwell Publishing Ltd

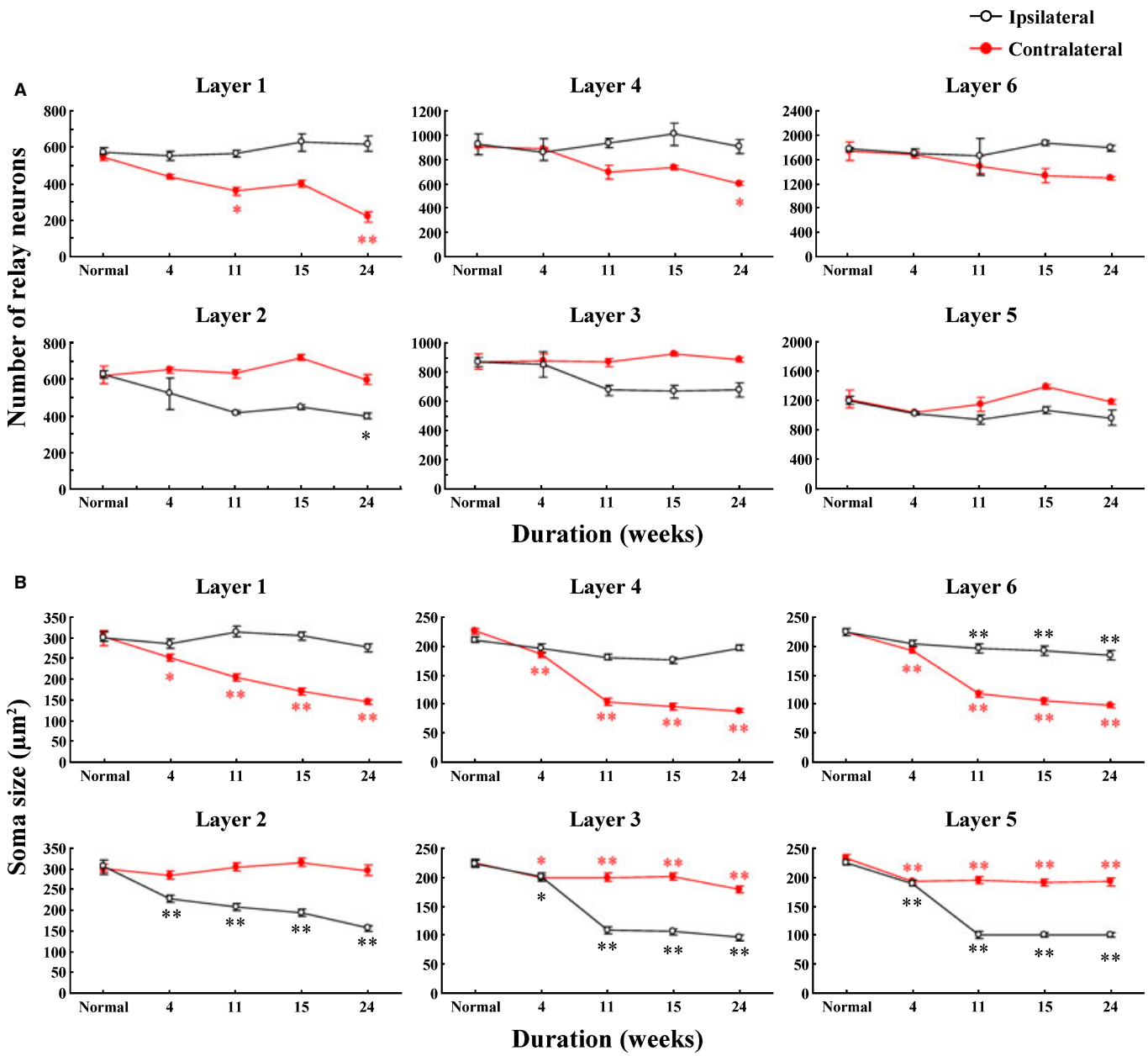

FIG. 3. (A) Prolonged elevation of IOP resulted in neuron loss in layers 1 and 4 on the contralateral side and layer 2 on the ipsilateral side at 11 and/or 24 weeks after the laser photocoagulation treatment and (B) neuron shrinkage in layers 1, 4 and 6 on the contralateral side and layers 2, 3 and 5 on the ipsilateral side at 4 weeks after the laser photocoagulation treatment. Values are the mean ± SEM (*$P < 0.05$, **$P < 0.01$ vs. normal; two-way ANOVA with Bonferroni adjustment).

layers 2 (magnocellular layer), 3 and 5 (parvocellular layer), and as predicted, neuronal losses were confirmed in these layers (Fig. 2A).

To compare cell numbers and the size distributions of parvalbumin-positive relay neurons in each layer of the LGN between the contralateral and ipsilateral sides, the area of parvalbumin-positive relay neurons was measured. ANOVAs to assess changes in the numbers of parvalbumin-positive relay neurons in the LGN revealed significant effects of side (layer 1: $F_{1,20} = 118.1$, $P < 0.001$; layer 2: $F_{1,20} = 55.8$, $P < 0.001$; layer 3: $F_{1,20} = 27.7$, $P < 0.001$; layer 4: $F_{1,20} = 63.4$, $P < 0.001$; layer 5: $F_{1,20} = 13.1$, $P = 0.002$; layer 6: $F_{1,20} = 13.5$, $P = 0.002$), significant effects of time (layer 1: $F_{4,20} = 6.8$, $P = 0.001$; layer 2: $F_{4,20} = 4.4$, $P = 0.011$; layer 4: $F_{4,20} = 7.4$, $P = 0.001$; layer 5: $F_{4,20} = 4.2$, $P = 0.013$), but not for layer 3 ($F_{4,20} = 2.8$, $P = 0.056$) or layer 6 ($F_{4,20} = 1.2$, $P = 0.327$) and significant interaction effects (layer 1: $F_{4,20} = 12.0$, $P < 0.001$; layer 2: $F_{4,20} = 5.0$, $P = 0.006$; layer 3: $F_{4,20} = 3.9$, $P = 0.017$; layer 4: $F_{4,20} = 11.5$, $P < 0.001$), but not for layer 5 ($F_{4,20} = 2.0$, $P = 0.134$) or layer 6 ($F_{4,20} = 2.6$, $P = 0.067$). ANOVAs for the mean parvalbumin-positive relay neuron size in the LGN also revealed significant effects of side (layer 1: $F_{1,990} = 224.4$, $P < 0.001$; layer 2: $F_{1,990} = 183.1$, $P < 0.001$; layer 3: $F_{1,990} = 209.8$, $P < 0.001$; layer 4: $F_{1,990} = 404.3$, $P < 0.001$; layer 5: $F_{1,990} = 272.1$, $P < 0.001$; layer 6: $F_{1,990} = 214.8$, $P < 0.001$) and significant effects of time (layer 1: $F_{4,990} = 25.5$, $P < 0.001$; layer 2: $F_{4,990} = 20.6$, $P < 0.001$; layer 3: $F_{4,990} = 116.9$, $P < 0.001$; layer 4: $F_{4,990} = 97.6$, $P < 0.001$; layer 5: $F_{4,990} = 93.5$, $P < 0.001$; layer 6: $F_{4,990} = 92.8$, $P < 0.001$) as well as significant interaction effects (layer 1: $F_{4,990} = 28.4$, $P < 0.001$; layer 2: $F_{4,990} = 18.4$, $P < 0.001$; layer 3: $F_{4,990} = 36.1$, $P < 0.001$; layer 4:

© 2011 The Authors. European Journal of Neuroscience © 2011 Federation of European Neuroscience Societies and Blackwell Publishing Ltd

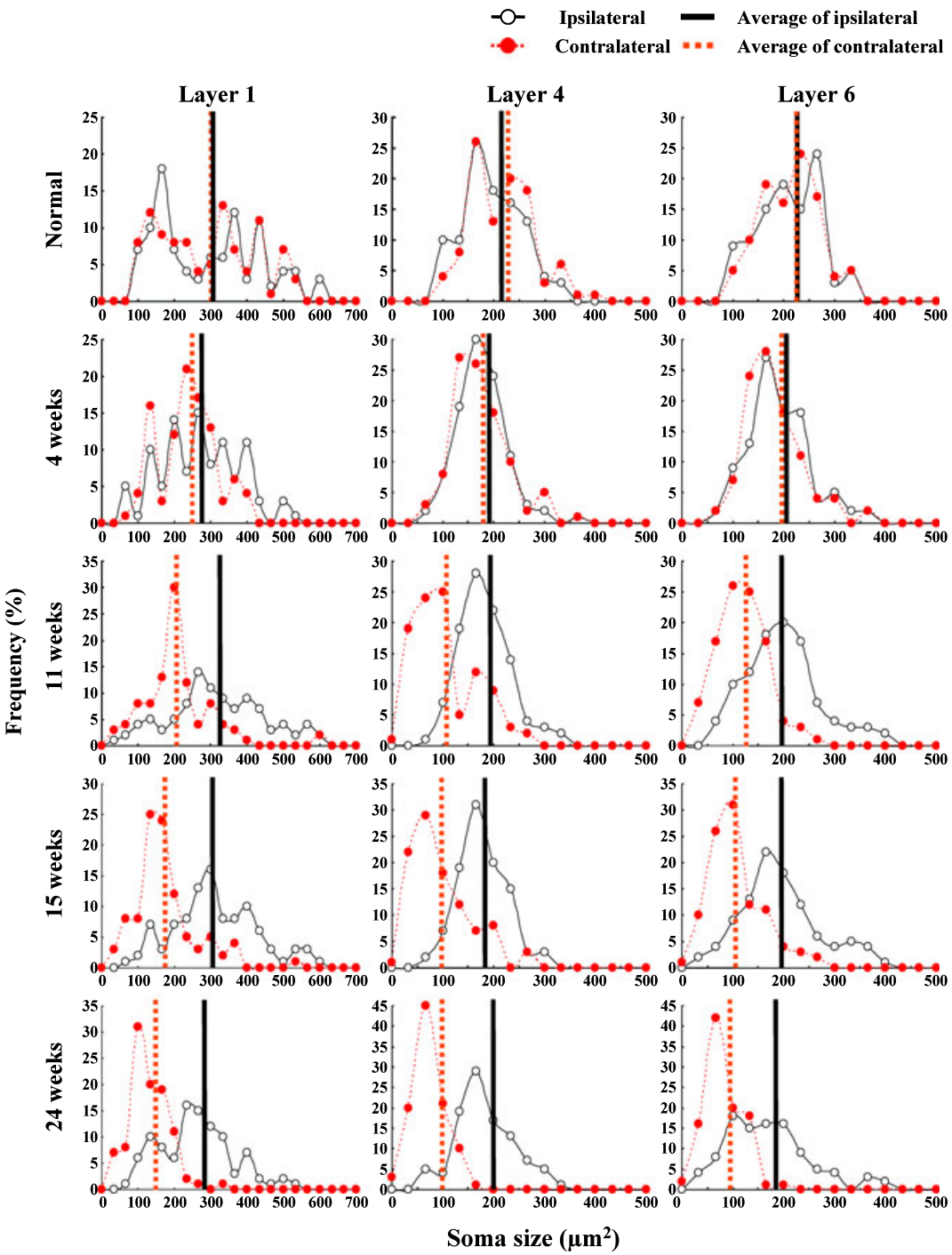

FIG. 4. Frequency distribution histograms compariing neuronal cell size in the LGN (layers 1, 4 and 6) between normal monkey and in those 4–24 weeks after the laser photocoagulation treatment. Layers 1, 4 and 6 on the contralateral side receive their innervations from the glaucomatous (left) eye, whereas layers 1, 4 and 6 on the ipsilateral side receive their retinal inputs from the non-treated control (right) eye. The neuronal cell-size distributions for layers 1, 4 and 6 on the contralateral side at 4–24 weeks after the laser photocoagulation treatment shifted further toward smaller particle sizes than those obtained for the normal monkey. For all comparisons vs. ipsilateral side – Kolmogorov–Smirnov test; $P < 0.0001$, except normal and 4-week samples.

$F_{4,990} = 79.7$, $P < 0.001$; layer 5: $F_{4,990} = 36.7$, $P < 0.001$; layer 6: $F_{4,990} = 28.6$, $P < 0.001$). The numbers of parvalbumin-positive relay neurons in layers 1, 4 and 6 of the contralateral LGN were 101.4, 88.0, 65.2, 56.3 and 53.2% in layer 1, 106.7, 94.3, 57.1, 54.3 and 45.2% in layer 4, and 100.0, 94.3, 60.0, 54.9 and 52.8% in layer 6 [normal, at 4, 11, 15 and 24 weeks after the laser photocoagulation treatment, respectively (vs. ipsilateral)] (Figs 2B and 3A). On the contralateral side, the mean parvalbumin-positive relay neuron size decreased to 95.3, 79.4, 63.6, 63.9 and 35.8% in layer 1, 98.0, 103.1, 74.3, 72.8 and 66.5% in layer 4, and 98.2, 98.6, 89.3, 70.9 and 72.1% in layer 6 [normal, at 4, 11, 15 and 24 weeks after the laser photocoagulation treatment, respectively (vs. ipsilateral)] (Figs 2B, 3B and 4). In layers 2, 3 and 5 on the ipsilateral side, the numbers of parvalbumin-positive relay neurons were 104.3, 88.2, 66.1, 61.9 and 66.7% in layer 2,

© 2011 The Authors. European Journal of Neuroscience © 2011 Federation of European Neuroscience Societies and Blackwell Publishing Ltd

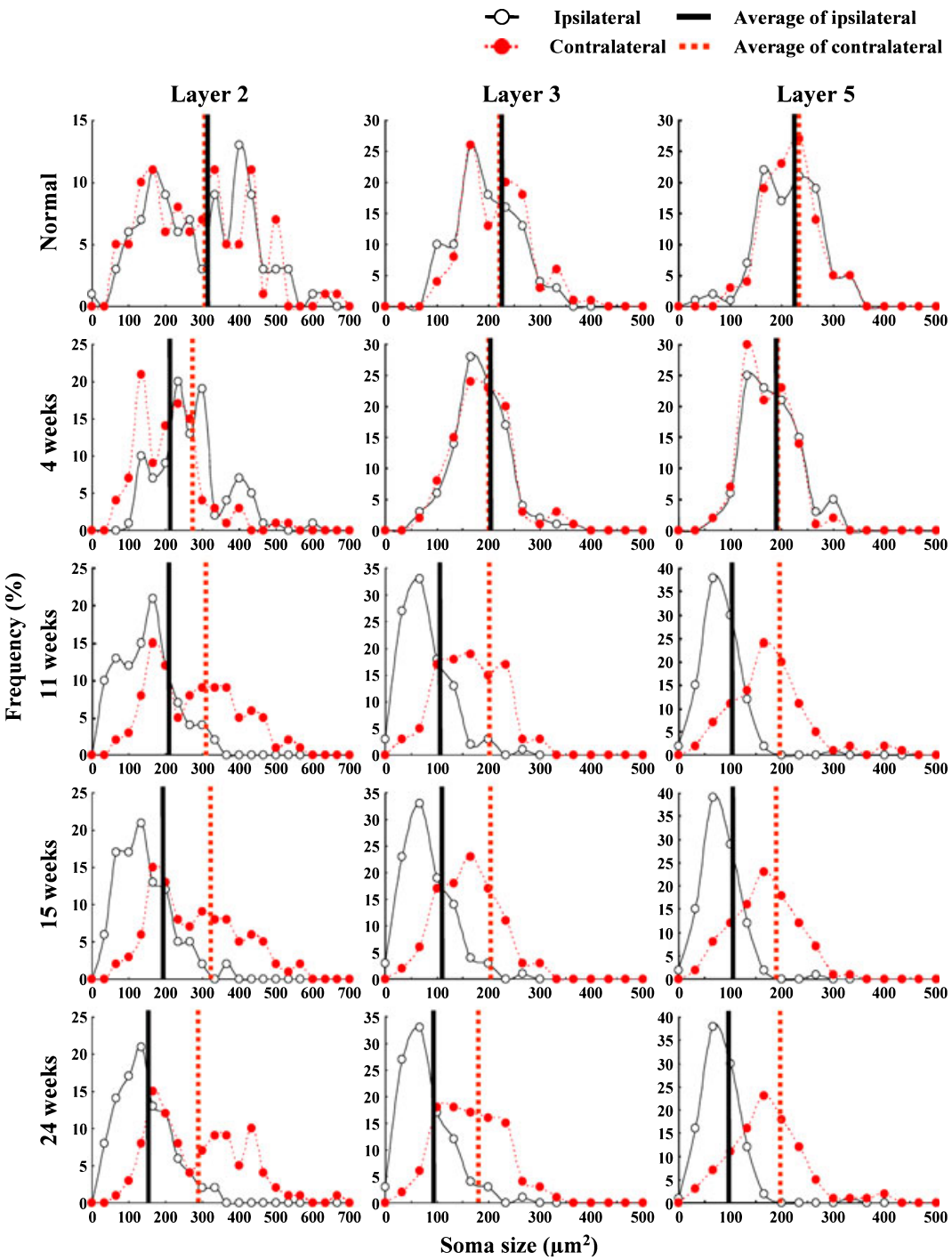

FIG. 5. Frequency distribution histograms comparing neuronal cell size in the LGN (layers 2, 3 and 5) between normal monkey and those at 4–24 weeks after the laser photocoagulation treatment. Layers 2, 3 and 5 on the ipsilateral side receive their innervations from the glaucomatous (left) eye, whereas layers 2, 3 and 5 on the contralateral side receive their retinal inputs from the non-treated control (right) eye. The neuronal cell-size distributions for layers 2, 3 and 5 on the ipsilateral side at 4–24 weeks after the laser photocoagulation treatment shifted further toward smaller particle sizes than those obtained for the normal monkey. For all comparisons vs. contralateral side – Kolmogorov–Smirnov test; $P < 0.0001$, except normal and 4-week samples.

100.5, 97.3, 78.2, 72.5 and 76.3% in layer 3, and 101.2, 98.5, 82.1, 77.0 and 81.8% in layer 5 [normal, at 4, 11, 15, and 24 weeks after the laser photocoagulation treatment, respectively (vs. contralateral)] (Figs 2B and 3A). The mean size of parvalbumin-positive relay neurons decreased to 102.5, 79.6, 67.9, 61.5 and 59.2% in layer 2, 99.2, 101.7, 54.4, 52.4 and 53.5% in layer 3, and 96.6, 98.0, 51.5, 52.7 and 51.9% in layer 5 [normal, at 4, 11, 15 and 24 weeks after the laser photocoagulation treatment, respectively (vs. contralateral)] (Figs 2B, 3B, and 5).

TUNEL assay

We used a TUNEL assay to detect apoptotic cells in the LGN after the laser photocoagulation treatment. Figure 6A shows representative

© 2011 The Authors. European Journal of Neuroscience © 2011 Federation of European Neuroscience Societies and Blackwell Publishing Ltd

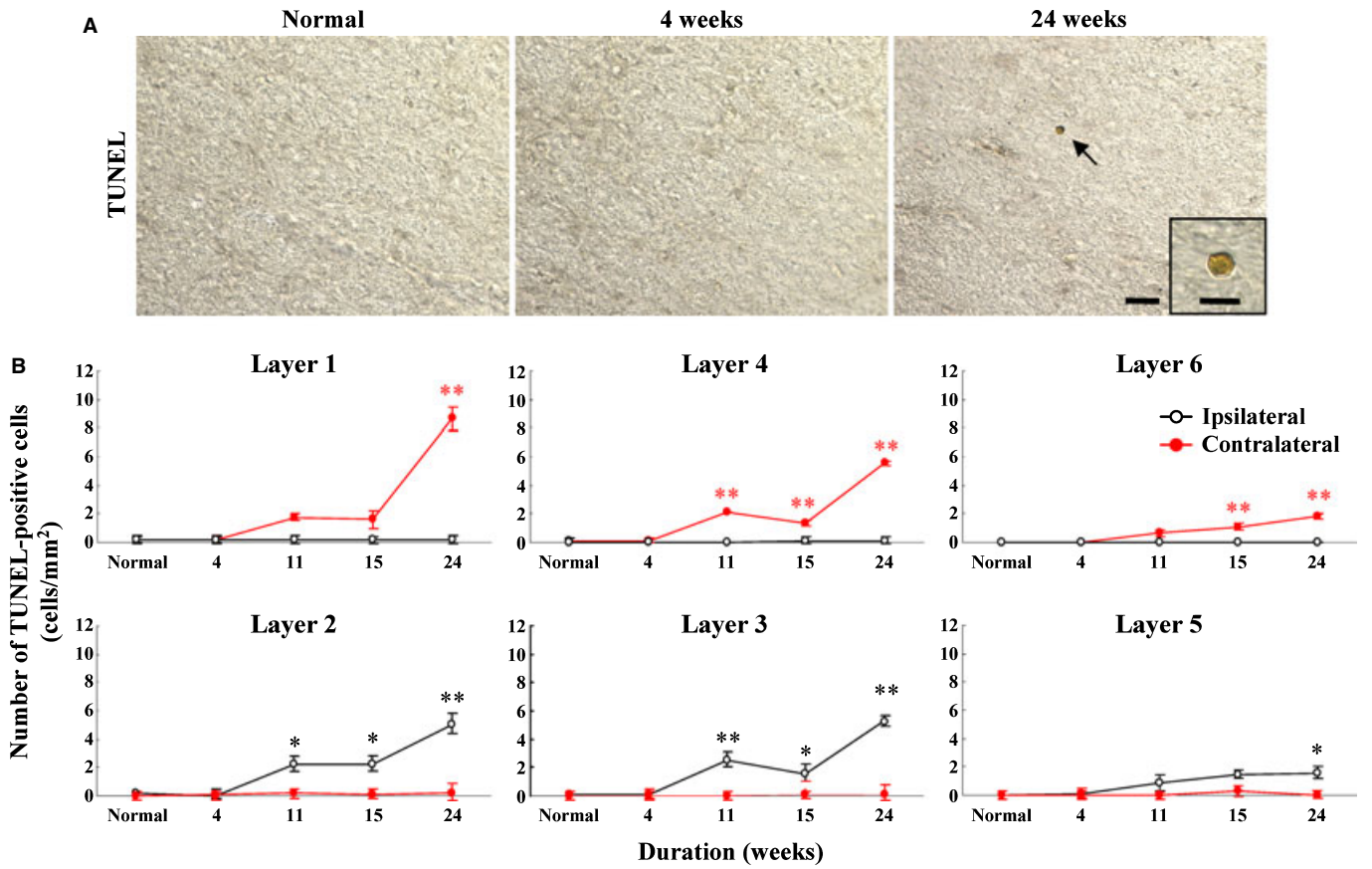

FIG. 6. (A) Representative micrographs showing TUNEL staining sections of layer 1 on the contralateral side from the normal monkey and monkeys that had the pressure in their left eye elevated for 4 and 24 weeks. Scale bar = 20 μm. Boxed areas are shown at higher magnification and horizontal scale bar is 10 μm. (B) TUNEL-positive cell density in each layer of the LGN at 4–24 weeks after the laser photocoagulation treatment. Values are the mean ± SEM (*$P < 0.05$, **$P < 0.01$ vs. Normal; two-way ANOVA with Bonferroni adjustment).

micrographs of the TUNEL-positive cell at layer 1 of the LGN at 24 weeks after IOP elevation. ANOVAs to assess changes in the density of TUNEL-positive cells revealed significant effects of side (layer 1: $F_{1,20} = 100.3$, $P < 0.001$; layer 2: $F_{1,20} = 90.1$, $P < 0.001$; layer 3: $F_{1,20} = 201.9$, $P < 0.001$; layer 4: $F_{1,20} = 620.9$, $P < 0.001$; layer 5: $F_{1,20} = 23.0$, $P < 0.001$; layer 6: $F_{1,20} = 97.3$, $P < 0.001$) and significant effects of time (layer 1: $F_{4,20} = 46.3$, $P < 0.001$; layer 2: $F_{4,20} = 24.6$, $P < 0.001$; layer 3: $F_{4,20} = 56.1$, $P < 0.001$; layer 4: $F_{4,20} = 197.7$, $P < 0.001$; layer 5: $F_{4,20} = 4.8$, $P = 0.007$; layer 6: $F_{4,20} = 23.4$, $P < 0.001$) as well as significant interaction effects (layer 1: $F_{4,20} = 46.6$, $P < 0.001$; layer 2: $F_{4,20} = 22.5$, $P < 0.001$; layer 3: $F_{4,20} = 51.3$, $P < 0.001$; layer 4: $F_{4,20} = 181.2$, $P < 0.001$; layer 5: $F_{4,20} = 3.7$, $P = 0.021$; layer 6: $F_{4,20} = 23.4$, $P < 0.001$). On the contralateral side, the density of TUNEL-positive cells increased to 1.8, 1.6 and 8.7 cells/mm^2 in layer 1, 2.1, 1.4 and 5.6 cells/mm^2 in layer 4, and 0.6, 1.1 and 1.9 cells/mm^2 in layer 6 at 11, 15 and 24 weeks after the laser photocoagulation treatment, respectively (that of the normal sample was 0.2, 0.1 and 0 cells/mm^2 in layers 1, 4 and 6, respectively; Fig. 6B). In layers 2, 3 and 5 on the ipsilateral side, the density of TUNEL-positive cells increased to 2.2, 2.2 and 5.1 cells/mm^2 in layer 2, 2.5, 1.5 and 5.3 cells/mm^2 in layer 3, and 0.9, 1.5 and 1.5 cells/mm^2 in layer 5 at 11, 15 and 24 weeks after the laser photocoagulation treatment, respectively (that of the normal sample was 0.1, 0.1 and 0 cells/mm^2 in layers 2, 3 and 5, respectively; Fig. 6B).

Expressions of ER stress-related protein

Next, we investigated the possible involvement of ER stress in LGN neuronal death after IOP elevation. Figure 7A shows representative micrographs of the polyubiquitin-positive cell at layer 1 of the LGN at 24 weeks after IOP elevation. ANOVAs to assess changes in the density of polyubiquitin-positive cells revealed significant effects of side (layer 1: $F_{1,20} = 111.7$, $P < 0.001$; layer 2: $F_{1,20} = 308.2$, $P < 0.001$; layer 3: $F_{1,20} = 114.5$, $P < 0.001$; layer 4: $F_{1,20} = 106.3$, $P < 0.001$; layer 5: $F_{1,20} = 124.6$, $P < 0.001$; layer 6: $F_{1,20} = 102.0$, $P < 0.001$) and significant effects of time (layer 1: $F_{4,20} = 20.6$, $P < 0.001$; layer 2: $F_{4,20} = 60.7$, $P < 0.001$; layer 3: $F_{4,20} = 22.0$, $P < 0.001$; layer 4: $F_{4,20} = 20.4$, $P < 0.001$; layer 5: $F_{4,20} = 26.6$, $P < 0.001$; layer 6: $F_{4,20} = 20.2$, $P < 0.001$) as well as significant interaction effects (layer 1: $F_{4,20} = 19.2$, $P < 0.001$; layer 2: $F_{4,20} = 58.8$, $P < 0.001$; layer 3: $F_{4,20} = 21.1$, $P < 0.001$; layer 4: $F_{4,20} = 19.9$, $P < 0.001$; layer 5: $F_{4,20} = 25.1$, $P < 0.001$; layer 6: $F_{4,20} = 19.1$, $P < 0.001$). On the contralateral side, the density of polyubiquitin-positive cells increased to 7.8, 6.0 and 6.3 cells/mm^2 in layer 1, 7.1, 5.4 and 4.1 cells/mm^2 in layer 4, and 3.5, 2.4 and 2.1 cells/mm^2 in layer 6 at 11, 15 and 24 weeks after the laser photocoagulation treatment, respectively (that of the normal sample was 0, 0 and 0 cells/mm^2 in layers 1, 4 and 6, respectively; Fig. 7B). In layers 2, 3 and 5 on the ipsilateral side, the density of polyubiquitin-positive cells increased to 7.9, 7.2 and 4.3 cells/mm^2 in layer 2, 6.7, 5.6 and 4.1 cells/mm^2 in layer 3, and

© 2011 The Authors. European Journal of Neuroscience © 2011 Federation of European Neuroscience Societies and Blackwell Publishing Ltd

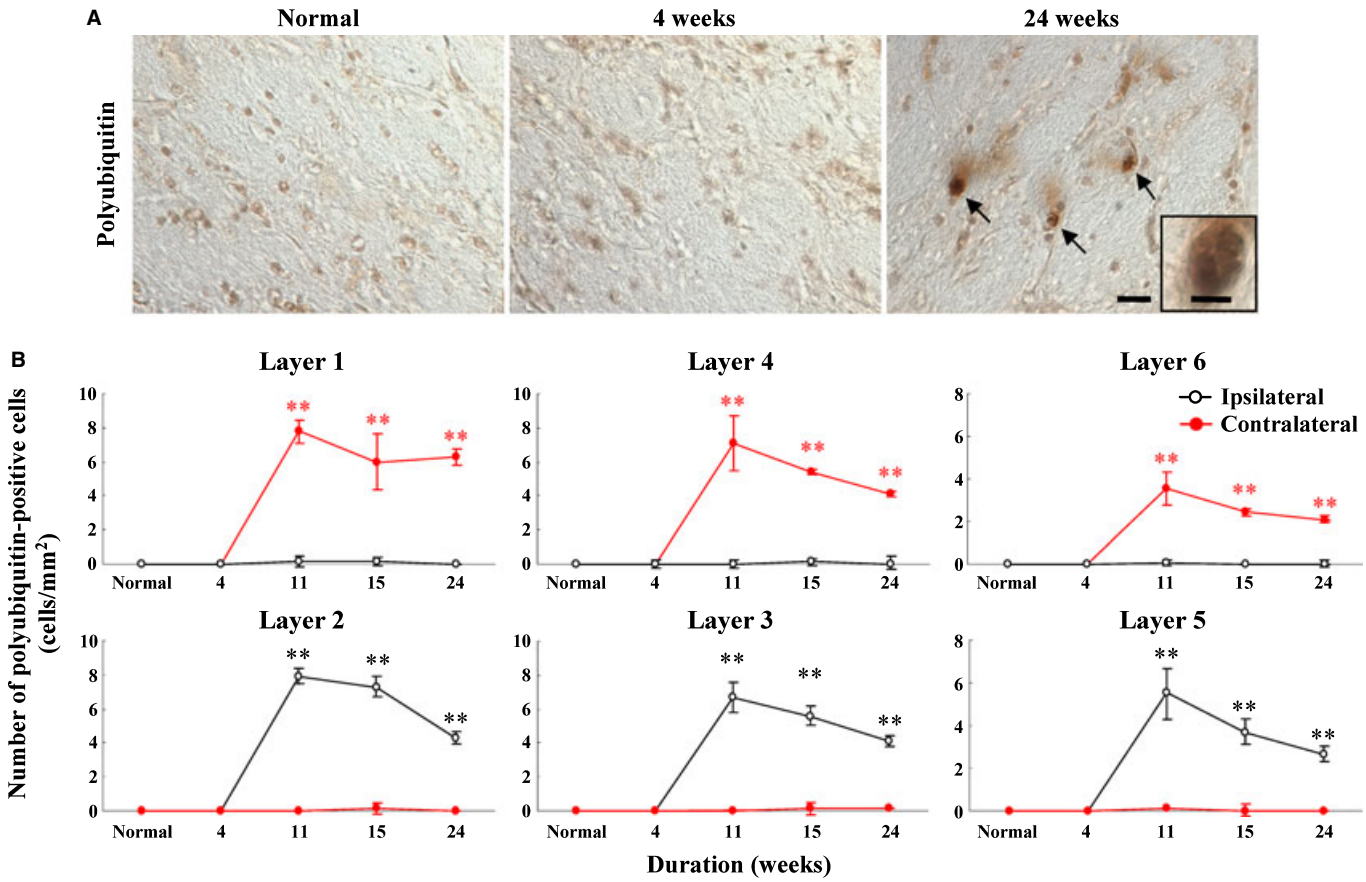

FIG. 7. (A) Representative micrographs showing polyubiquitin-stained sections of layer 1 on the contralateral side from the normal monkey and monkeys that had the pressure in their left eye elevated for 4 and 24 weeks. Scale bar = 20 μm. Boxed areas are shown at higher magnification and horizontal scale bar is 10 μm. (B) Polyubiquitin-positive cell density at each layers of the LGN at 4–24 weeks after the laser photocoagulation treatment. Value are the mean ± SEM (**$P < 0.01$ vs. Normal; two-way ANOVA with Bonferroni adjustment).

5.5, 3.7 and 2.7 cells/mm^2 in layer 5 at 11, 15 and 24 weeks after the laser photocoagulation treatment, respectively (that of the normal sample was 0, 0 and 0 cells/mm^2 in layers 2, 3 and 5, respectively) (Fig. 7B).

Figure 8A also shows representative micrographs of the p-eIF2α-positive cell at layer 1 of the LGN at 24 weeks after IOP elevation. ANOVAs to assess changes in the density of p-eIF2α-positive-positive cells revealed significant effects of side (layer 1: $F_{1,20} = 114.2$, $P < 0.001$; layer 2: $F_{1,20} = 166.6$, $P < 0.001$; layer 3: $F_{1,20} = 41.7$, $P < 0.001$; layer 4: $F_{1,20} = 24.7$, $P < 0.001$; layer 5: $F_{1,20} = 177.1$, $P < 0.001$; layer 6: $F_{1,20} = 23.0$, $P < 0.001$) and significant effects of time (layer 1: $F_{4,20} = 40.4$, $P < 0.001$; layer 2: $F_{4,20} = 36.4$, $P < 0.001$; layer 3: $F_{4,20} = 15.6$, $P < 0.001$; layer 4: $F_{4,20} = 10.1$, $P < 0.001$; layer 5: $F_{4,20} = 59.1$, $P < 0.001$; layer 6: $F_{4,20} = 11.7$, $P < 0.001$) as well as significant interaction effects (layer 1: $F_{4,20} = 39.4$, $P < 0.001$; layer 2: $F_{4,20} = 34.3$, $P < 0.001$; layer 3: $F_{4,20} = 15.5$, $P < 0.001$; layer 4: $F_{4,20} = 10.1$, $P < 0.001$; layer 5: $F_{4,20} = 55.5$, $P < 0.001$; layer 6: $F_{4,20} = 11.14$, $P < 0.001$). On the contralateral side, the density of p-eIF2α-positive cells increased to 6.8, 4.8 and 20.2 cells/mm^2 in layer 1, 5.5, 2.7 and 17.2 cells/mm^2 in layer 4, and 2.3, 1.6 and 11.1 cells/mm^2 in layer 6 at 11, 15 and 24 weeks after the laser photocoagulation treatment, respectively (that of the normal sample was 0.2, 0 and 0 cells/mm^2 in layers 1, 4, and 6 respectively) (Fig. 8B). In layers 2, 3 and 5 on the ipsilateral side, the density of p-eIF2α-positive cells increased to 7.7, 5.6 and 11.7 cells/mm^2 in layer 2, 6.0, 3.0 and 16.7 cells/mm^2 in layer 3, and 4.3, 2.5 and 9.9 cells/mm^2 in layer 5 at 11, 15 and 24 weeks after the laser photocoagulation treatment, respectively (that of the normal sample was 0.2, 0.1 and 0 cells/mm^2 in layers 2, 3 and 5, respectively; Fig. 8B).

Figure 9A also shows representative micrographs of the CHOP-positive cell at layer 1 of the LGN at 24 weeks after IOP elevation. ANOVAs to assess changes in the density of CHOP-positive-positive cells revealed significant effects of side (layer 1: $F_{1,20} = 25.8$, $P < 0.001$; layer 2: $F_{1,20} = 77.4$, $P < 0.001$; layer 3: $F_{1,20} = 309.7$, $P < 0.001$; layer 4: $F_{1,20} = 157.2$, $P < 0.001$; layer 5: $F_{1,20} = 159.4$, $P < 0.001$; layer 6: $F_{1,20} = 102.3$, $P < 0.001$) and significant effects of time (layer 1: $F_{4,20} = 14.6$, $P < 0.001$; layer 2: $F_{4,20} = 31.1$, $P < 0.001$; layer 3: $F_{4,20} = 102.1$, $P < 0.001$; layer 4: $F_{4,20} = 54.6$, $P < 0.001$; layer 5: $F_{4,20} = 55.7$, $P < 0.001$; layer 6: $F_{4,20} = 40.4$, $P < 0.001$) as well as significant interaction effects (layer 1: $F_{4,20} = 14.4$, $P < 0.001$; layer 2: $F_{4,20} = 28.6$, $P < 0.001$; layer 3: $F_{4,20} = 94.6$, $P < 0.001$; layer 4: $F_{4,20} = 50.9$, $P < 0.001$; layer 5: $F_{4,20} = 52.8$, $P < 0.001$; layer 6: $F_{4,20} = 38.9$, $P < 0.001$). On the contralateral side, the density of CHOP-positive cells increased to 2.8, 2.8 and 17.9 cells/mm^2 in layer 1, 2.8, 4.2 and 11.3 cells/mm^2 in layer 4, and 1.3, 2.0 and 6.3 cells/mm^2 in layer 6 at 11, 15 and 24 weeks after the laser photocoagulation treatment, respectively (that of the normal sample was 0, 0 and 0 cells/mm^2 in layers 1, 4 and 6, respectively; Fig. 9B). In layers 2, 3 and 5 on the ipsilateral side, the density of CHOP-positive cells increased to 2.9, 2.7 and 10.4 cells/mm^2 in layer 2, 3.0, 4.4 and 11.1 cells/mm^2 in layer 3, and 2.1, 3.0

© 2011 The Authors. European Journal of Neuroscience © 2011 Federation of European Neuroscience Societies and Blackwell Publishing Ltd

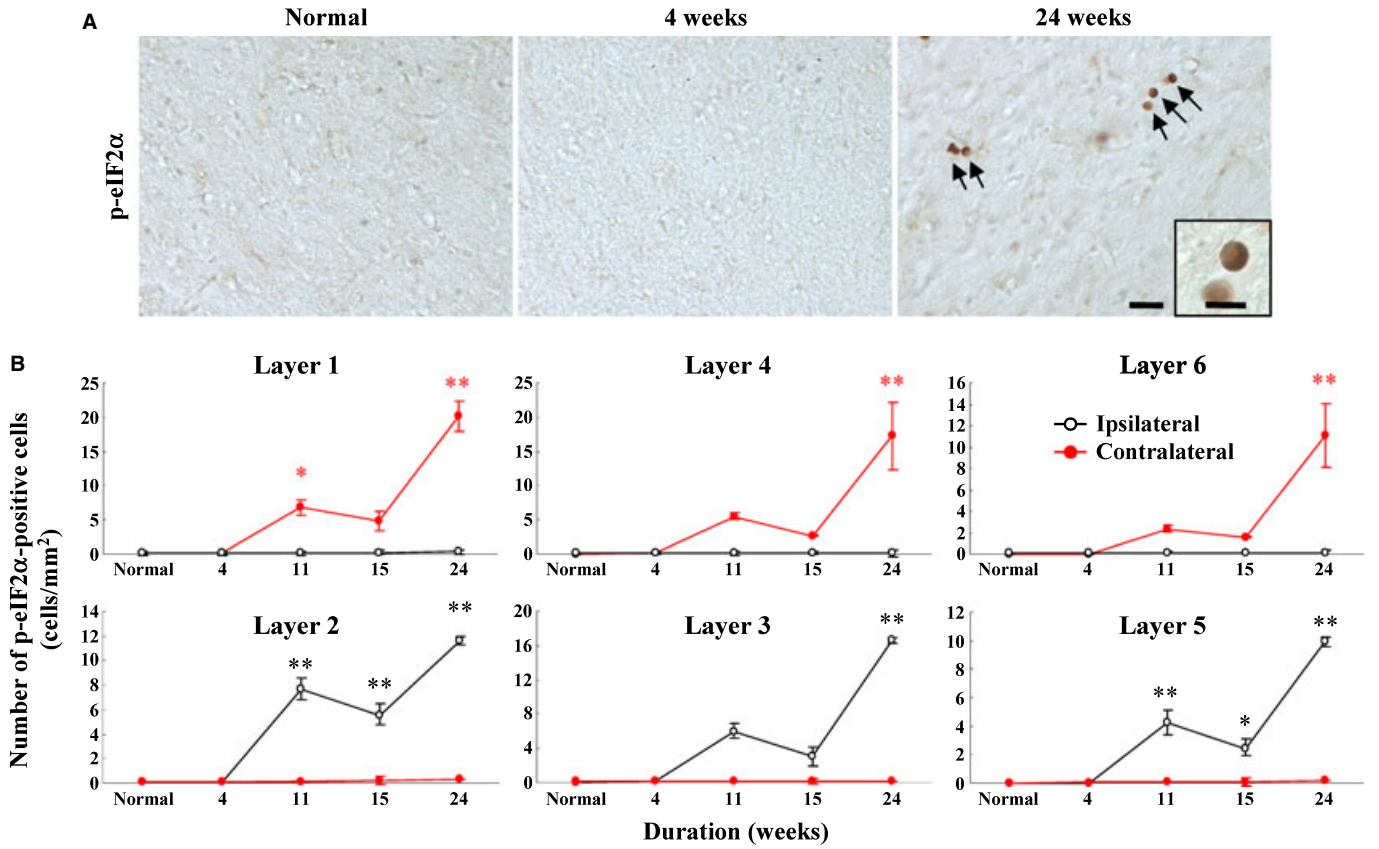

FIG. 8. (A) Representative micrographs showing p-eIF2α-stained sections of layer 1 on the contralateral side from the normal monkey and monkeys that had the pressure in their left eye elevated for 4 and 24 weeks. Scale bar = 20 μm. Boxed areas are shown at higher magnification and horizontal scale bar is 10 μm. (B) p-eIF2α-positive cell density in each layer of the LGN at 4–24 weeks after the laser photocoagulation treatment. Values are the mean ± SEM (*$P < 0.05$, **$P < 0.01$ vs. Normal; two-way ANOVA with Bonferroni adjustment).

and 8.5 cells/mm^2 in layer 5 at 11, 15 and 24 weeks after the laser photocoagulation treatment, respectively (that of the normal sample was 0, 0 and 0 cells/mm^2 in layers 2, 3 and 5, respectively; Fig. 9B).

Double immunofluorescence

To identify p-eIF2α- and CHOP-positive cells, double immunofluorescence was performed for parvalbumin and p-eIF2α or CHOP in the LGN after IOP elevation, Fig. 10 shows representative micrographs of layer 1 of the contralateral LGN double-immunostained with parvalbumin and p-eIF2α or CHOP at 24 weeks after IOP elevation. Parvalbumin-positive relay neurons in layers 1, 4 and 6 of the contralateral LGN were found to express p-eIF2α and CHOP at 24 weeks after the laser photocoagulation treatment.

Discussion

In the present study, loss of parvalbumin-positive relay neurons and/or neuronal atrophy in the LGN layers connected to the eye were shown at 4–24 weeks after IOP elevation. In these LGN regions, TUNEL-positive cells, polyubiquitinated proteins and ER stress-related proteins were also observed at 11–24 weeks after IOP elevation. In agreement with our previous data (Ito *et al.*, 2009a), the loss of LGN neurons was preceded by loss of RGC axons after IOP elevation in the present study.

Recently, ER stress has been suggested to be involved in neurodegenerative diseases, including glaucoma (Shimazawa *et al.*, 2007b; Inokuchi *et al.*, 2009; Doh *et al.*, 2010). Indeed, both our previous study and another report have suggested that the average number of RGCs decreased significantly and TUNEL-positive cells and the production of ER stress-related proteins were detected in the ganglion cell layer of retina in mouse and rat glaucoma models (Shimazawa *et al.*, 2007a; Doh *et al.*, 2010). In these models, ER stress-induced RGC death via the p-eIF2α/CHOP signal pathway occurred after IOP elevation (Shimazawa *et al.*, 2007a; Doh *et al.*, 2010). However, the precise pathobiology of LGN neuronal degeneration in glaucoma remains unknown.

In the LGN, the relay neurons predominately express the *N*-methyl-D-aspartic acid (NMDA – an excitatory amino acid) receptor (Salt, 1986, 1987; Scharfman *et al.*, 1990; Jones *et al.*, 1998). In glaucoma models, excessive activation of this receptor leads to an overload of intracellular Ca^{2+} (Yücel *et al.*, 2006; Ito *et al.*, 2008). Such elevations in Ca^{2+} elicit the activation of nitric oxide (NO) formation through NO synthase activation (Lipton *et al.*, 1994; Wang *et al.*, 2000; Nucci *et al.*, 2003; Uehara *et al.*, 2006). NO induces S-nitrosylation of protein disulfide isomerase, a luminal enzyme of the ER, and inhibits its enzymatic activity (Uehara *et al.*, 2006). As a consequence, this leads to excess accumulation of misfolded or unfolded proteins within the ER that may lead to ER stress-induced cell death via the p-eIF2α/CHOP signal pathway (Ilieva *et al.*, 2007; Okada *et al.*, 2005; Uehara *et al.*, 2006; Kim *et al.*, 2008). The involvement of ER stress in relay neuronal atrophy and death within the LGN via the NMDA-

© 2011 The Authors. European Journal of Neuroscience © 2011 Federation of European Neuroscience Societies and Blackwell Publishing Ltd

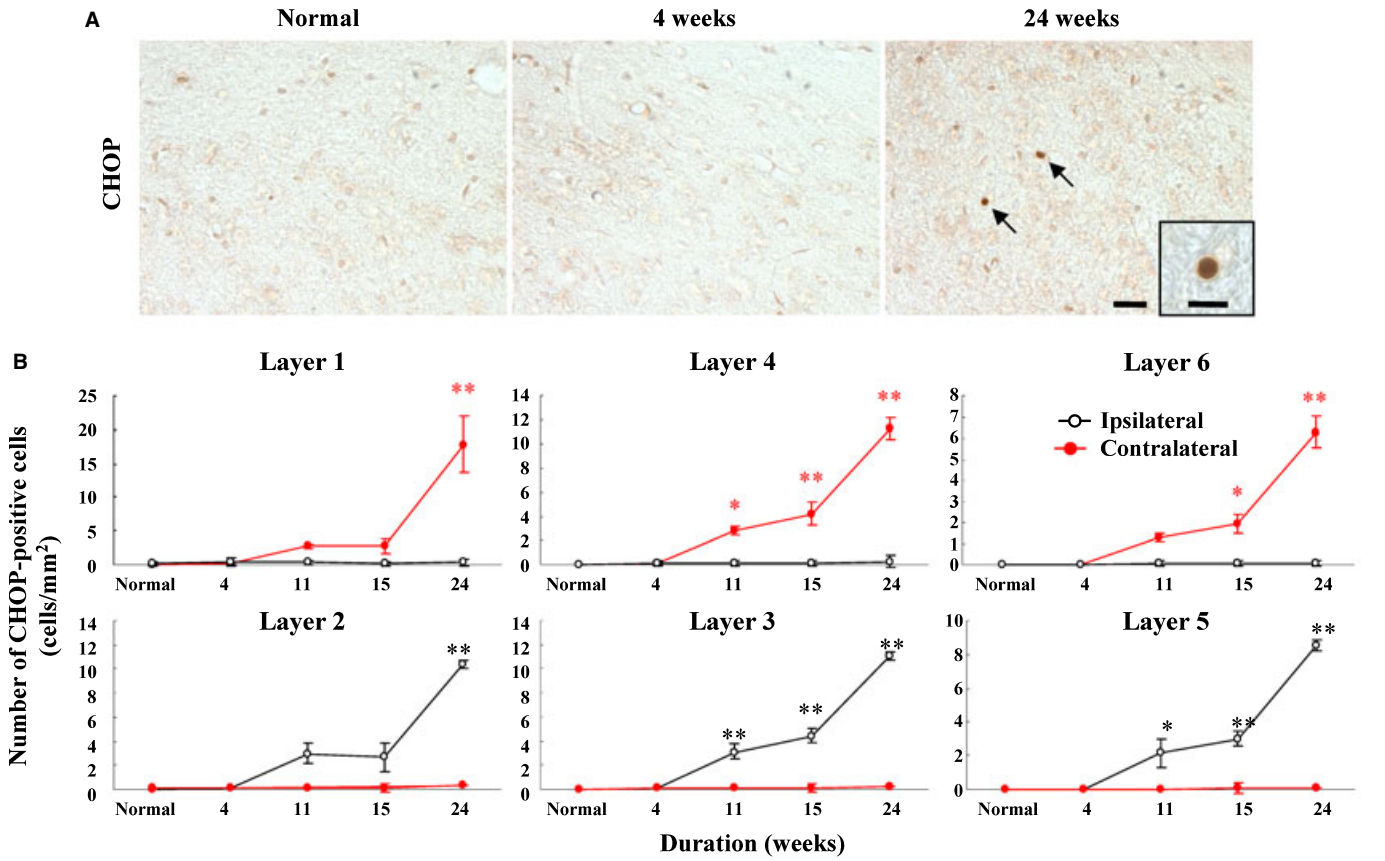

FIG. 9. (A) Representative micrographs showing CHOP-stained sections of layer 1 on the contralateral side from the normal monkey and monkeys that had the pressure in their left eye elevated for 4 and 24 weeks. Scale bar = 20 μm. Boxed areas are shown at higher magnification and horizontal scale bar is 10 μm. (B) CHOP-positive cell density in each layer of the LGN at 4–24 weeks after the laser photocoagulation treatment. Values are the mean ± SEM (*$P < 0.05$, **$P < 0.01$ vs. Normal; two-way ANOVA with Bonferroni adjustment).

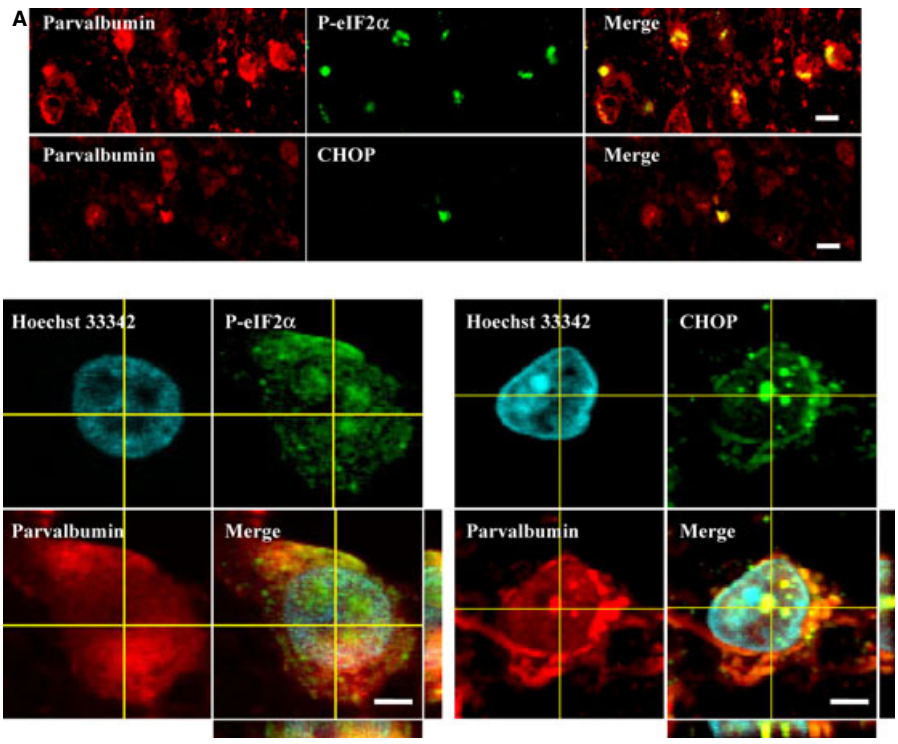

FIG. 10. Immunolocalizations of p-eIF2α and CHOP in the LGN. (A) Representative micrographs showing parvalbumin/CHOP double-immunostaining from monkeys at 24 weeks after the laser photocoagulation treatment showing sections of layer 1 on the contralateral side. Scale bar = 20 μm. (B) Immunostained sections analysed by confocal microscopy. Scale bar = 3 μm.

© 2011 The Authors. European Journal of Neuroscience © 2011 Federation of European Neuroscience Societies and Blackwell Publishing Ltd

Ca^{2+} – NO synthase/NO pathway after IOP elevation supports our results. In fact, in our previous studies, memantine, an NMDA antagonist, and lomerizine, a Ca^{2+} channel blocker, reduced neuronal atrophy in the LGN after retinal damage (Ito *et al.*, 2008, Ito *et al.*, 2010). To our knowledge, monocular deprivation causes apoptosis via glutamate signaling and NO production in the LGN (Nucci *et al.*, 2003). Furthermore, the above studies were performed using mice and rats, but not primates, to investigate whether ER stress was involved in the LGN degeneration after glaucomatous RGC death. Therefore, this is the first report of TUNEL-positive apoptotic cells and the production of ER stress-related proteins being detected in LGN neurons after IOP elevation in monkeys.

Regarding the localization of ER stress-related proteins, parvalbumin-positive relay neurons in the LGN layers connected to the eye with elevated IOP were found to express p-eIF2α and CHOP at 11–24 weeks after IOP elevation in the present study. Delayed neuronal death in these regions progressed gradually following RGC axon loss by IOP elevation (Table 2). As expression of the ER stress-related proteins measured here may be detected before dying cells at each sampling point (i.e. at 4, 11, 15 and 24 weeks after IOP elevation), the number of cells positive for ER stress markers may be relatively low in comparison with the number (and extent) of parvalbumin-positive relay neuron loss in the LGN. The total number of detectable neuron loss in the LGN, but not cells positive for ER stress markers, increased during the study period. Therefore, the number of ER stress-positive cells in the LGN at each sampling point may be smaller than those undergoing neuronal cell death. In this context, it is noteworthy that the timing of the up-regulation of p-eIF2α and CHOP proteins coincided with the timing of the decrease in neuronal cells during the study period (Figs 3, 8 and 9) and these ER stress-related proteins were co-localized with parvalbumin-positive relay neurons (Fig. 10). Furthermore, the increase in polyubiquitinated proteins was preceded by an increase in TUNEL-positive cells in the LGN after the laser photocoagulation treatment during the study period (Figs 6 and 7). These findings indicate that excessive ER stress (caused by accumulation of misfolded or unfolded proteins) induces LGN neuronal death via the activation of the ER-dependent apoptotic pathway, suggesting that the ER-stress pathway may play an important role in LGN neuronal death after IOP elevation.

On the other hand, an increase in glucose-regulated protein 78 (GRP78) was not detected in the LGN after IOP elevation during the study period as assessed by immunohistochemistry (data not shown). A possible explanation for this observation is a direct cytotoxic effect of p-eIF2α (Srivastava *et al.*, 1998) and activation of the caspase-3 pathway (Martin *et al.*, 2001, 2003; Repici *et al.*, 2003), whereby p-eIF2α directly mediates apoptosis in response to activation of the double-stranded RNA-dependent protein kinase (PKR). In fact, we have previously shown that inhibition of PKR activation was neuroprotective against ER stress-induced RGC death (Shimazawa *et al.*, 2007b). Although GFP78 expression requires further studies, the present data suggest that impaired induction of anti-apoptotic GRP78 is accompanied by a strong induction of pro-apoptotic signal in the ER, indicating a signal imbalance leaning toward cell death. We have previously shown that a preferential inducer of GRP78 exhibited the potential to be a therapeutic agent for ER stress-induced retinal diseases (Kudo *et al.*, 2008; Oida *et al.*, 2008; Inokuchi *et al.*, 2009).

In conclusion, the present study indicates that ER stress may be involved in LGN neuronal death after IOP elevation, and the up-regulation of p-eIF2α and CHOP protein levels in the parvalbumin-positive relay neurons may play roles in the cell death process induced by high IOP in monkey. These findings also indicate that ER stress induced by retinal damage may play a pivotal role in the pathogenesis of the blindness caused by retinal diseases such as glaucoma.

Acknowledgements

This study was supported in part by Grants-in-Aid for Scientific Research (C) (nos. 20592082 and 21592262) and Scientific Research (B) (No. 22390321) from the Ministry of Education, Culture, Sports, Science, and Technology, Japan, by a Grant-in-Aid from the Japan Society for the Promotion of Science (no. 20.10786), by Takada Science Foundation, and by consignment expenses from the Molecular Imaging Program on the 'Research Base for Exploring New Drugs' [Ministry of Education, Culture, Sports, Science and Technology (MEXT), Japan].

Abbreviations

CHOP, C/EBP-homologous protein; ER, endoplasmic reticulum; IOP, intraocular pressure; LGN, lateral geniculate nucleus; NMDA, *N*-methyl-D-aspartic acid; NO, nitric oxide; p-eIF2α, phosphorylation of eukaryotic initiation factor 2α; RGC, retinal ganglion cell; TUNEL, terminal deoxynucleotidyl transferase-mediated dUTP nick end labeling.

References

Aridor, M. & Balch, W.E. (1999) Integration of endoplasmic reticulum signaling in health and disease. *Nat. Med.*, **5**, 745–751.

Doh, S.H., Kim, J.H., Lee, K.M., Park, H.Y. & Park, C.K. (2010) Retinal ganglion cell death induced by endoplasmic reticulum stress in a chronic glaucoma model. *Brain Res.*, **1308**, 158–166.

Gupta, N. & Yücel, Y.H. (2003) Brain changes in glaucoma. *Eur. J. Ophthalmol.*, **13**, S32–S35.

Harding, H.P., Calfon, M., Urano, F., Novoa, I. & Ron, D. (2002) Transcriptional and translational control in the Mammalian unfolded protein response. *Annu. Rev. Cell Dev. Biol.*, **18**, 575–599.

Ilieva, E.V., Ayala, V., Jové, M., Dalfó, E., Cacabelos, D., Povedano, M., Bellmunt, M.J., Ferrer, I., Pamplona, R. & Portero-Otín, M. (2007) Oxidative and endoplasmic reticulum stress interplay in sporadic amyotrophic lateral sclerosis. *Brain*, **130**, 3111–3123.

Inokuchi, Y., Nakajima, Y., Shimazawa, M., Kurita, T., Kubo, M., Saito, A., Sajiki, H., Kudo, T., Aihara, M., Imaizumi, K., Araie, M. & Hara, H. (2009) Effect of an inducer of BiP, a molecular chaperone, on endoplasmic reticulum (ER) stress-induced retinal cell death. *Invest. Ophthalmol. Vis. Sci.*, **50**, 334–344.

Ito, Y., Nakamura, S., Tanaka, H., Shimazawa, M., Araie, M. & Hara, H. (2008) Memantine protects against secondary neuronal degeneration in lateral geniculate nucleus and superior colliculus after retinal damage in mice. *CNS Neurosci. Ther.*, **14**, 192–202.

Ito, Y., Shimazawa, M., Chen, Y.N., Tsuruma, K., Yamashima, T., Araie, M. & Hara, H. (2009a) Morphological changes in the visual pathway induced by experimental glaucoma in Japanese monkeys. *Exp. Eye Res.*, **89**, 246–255.

Ito, Y., Yamada, M., Tanaka, H., Aida, K., Tsuruma, K., Shimazawa, M., Hozumi, I., Inuzuka, T., Takahashi, H. & Hara, H. (2009b) Involvement of CHOP, an ER-stress apoptotic mediator, in both human sporadic ALS and ALS model mice. *Neurobiol. Dis.*, **36**, 470–476.

Ito Y., Nakamura, S., Tanaka, H., Tsuruma, K., Shimazawa, M., Araie, M. & Hara, H. (2010) Lomerizine, a Ca^{2+} channel blocker, protects against neuronal degeneration within the visual center of the brain after retinal damage in mice. *CNS Neurosci. Ther.* **16**, 103–114.

Johnson, J.K. & Casagrande, V.A. (1995) Distribution of calcium-binding proteins within parallel visual pathways of a primate. *J. Comp. Neurol.*, **356**, 238–260.

Jones, E.G. & Hendry, S.H. (1988) Differential calcium binding protein immunoreactivity distinguishes classes of relay neurons in monkey thalamic nuclei. *Eur. J. Neurosci.*, **1**, 222–246.

Jones, E.G., Tighilet, B., Tran, B.V. & Huntsman, M.M. (1998) Nucleus- and cell-specific expression of NMDA and non-NMDA receptor subunits in monkey thalamus. *J. Comp. Neurol.*, **397**, 371–393.

Kaufman, R.J. (1999) Stress signaling from the lumen of the endoplasmic reticulum: coordination of gene transcriptional and translational controls. *Genes Dev.*, **13**, 1211–1233.

© 2011 The Authors. European Journal of Neuroscience © 2011 Federation of European Neuroscience Societies and Blackwell Publishing Ltd

Kim, I., Xu, W. & Reed, J.C. (2008) Cell death and endoplasmic reticulum stress: disease relevance and therapeutic opportunities. *Nat. Rev. Drug Discov.*, **7**, 1013–1030.

Kudo, T., Kanemoto, S., Hara, H., Morimoto, N., Morihara, T., Kimura, R., Tabira, T., Imaizumi, K. & Takeda, M. (2008) A molecular chaperone inducer protects neurons from ER stress. *Cell Death Differ.*, **15**, 364–375.

Le Vay, S. (1971) On the neurons and synapses of the lateral geniculate nucleus of the monkey, and the effects of eye enucleation. *Z. Zellforsch. Mikrosk. Anat.*, **113**, 396–419.

Lipton, S.A., Singel, D.J. & Stamler, J.S. (1994) Nitric oxide in the central nervous system. *Prog. Brain Res.*, **103**, 359–364.

Martin, L.J., Kaiser, A., Yu, J.W., Natale, J.E. & Al-Abdulla, N.A. (2001) Injury-induced apoptosis of neurons in adult brain is mediated by p53-dependent and p53-independent pathways and requires Bax. *J. Comp. Neurol.*, **433**, 299–311.

Martin, L.J., Price, A.C., McClendon, K.B., Al-Abdulla, N.A., Subramaniam, J.R., Wong, P.C. & Liu, Z. (2003) Early events of target deprivation/axotomy-induced neuronal apoptosis in vivo: oxidative stress, DNA damage, p53 phosphorylation and subcellular redistribution of death proteins. *J. Neurochem.*, **85**, 234–247.

Nakamura, T. & Lipton, S.A. (2009) Cell death: protein misfolding and neurodegenerative diseases. *Apoptosis*, **14**, 455–468.

Nucci, C., Morrone, L., Rombolà, L., Nisticò, R., Piccirilli, S. & Cerulli, L. (2003) Multifaceted roles of nitric oxide in the lateral geniculate nucleus: from visual signal transduction to neuronal apoptosis. *Toxicol. Lett.*, **139**, 163–173.

Oida, Y., Izuta, H., Oyagi, A., Shimazawa, M., Kudo, T., Imaizumi, K. & Hara, H. (2008) Induction of BiP, an ER-resident protein, prevents the neuronal death induced by transient forebrain ischemia in gerbil. *Brain Res.*, **1208**, 217–224.

Okada, K., Minamino, T. & Kitakaze, M. (2005) Role of endoplasmic reticulum stress in hypertrophic and failing hearts. *Nippon Yakurigaku Zasshi*, **126**, 385–389.

Oyadomari, S. & Mori, M. (2004) Roles of CHOP/GADD153 in endoplasmic reticulum stress. *Cell Death Differ.*, **11**, 381–389.

Quigley, H.A. & Hohman, R.M. (1983) Laser energy levels for trabecular meshwork damage in the primate eye. *Invest. Ophthalmol. Vis. Sci.*, **24**, 1305–1307.

Repici, M., Atzori, C., Migheli, A. & Vercelli, A. (2003) Molecular mechanisms of neuronal death in the dorsal lateral geniculate nucleus following visual cortical lesions. *Neuroscience*, **117**, 859–867.

Resnikoff, S., Pascolini, D., Etya'ale, D., Kocur, I., Pararajasegaram, R., Pokharel, G.P. & Mariotti, S.P. (2004) Global data on visual impairment in the year 2002. *Bull. World Health Organ.*, **82**, 844–851.

Salt, T.E. (1986) Mediation of thalamic sensory input by both NMDA receptors and non-NMDA receptors. *Nature*, **322**, 263–265.

Salt, T.E. (1987) Excitatory amino acid receptors and synaptic transmission in the rat ventrobasal thalamus. *J. Physiol.*, **391**, 499–510.

Scharfman, H.E., Lu, S.M., Guido, W., Adams, P.R. & Sherman, S.M. (1990) *N*-methyl-D-aspartate receptors contribute to excitatory postsynaptic potentials of cat lateral geniculate neurons recorded in thalamic slices. *Proc. Natl Acad. Sci. USA*, **87**, 4548–4552.

Shimazawa, M., Inokuchi, Y., Ito, Y., Murata, H., Aihara, M., Miura, M., Araie, M. & Hara, H. (2007a) Involvement of ER stress in retinal cell death. *Mol. Vis.*, **13**, 578–587.

Shimazawa, M., Ito, Y., Inokuchi, Y. & Hara, H. (2007b) Involvement of double-stranded RNA-dependent protein kinase in ER stress-induced retinal neuron damage. *Invest. Ophthalmol. Vis. Sci.*, **48**, 3729–3736.

Somogyi, J., Eysel, U. & Hamori, J. (1987) A quantitative study of morphological reorganization following chronic optic deafferentation in the adult cat dorsal lateral geniculate nucleus. *J. Comp. Neurol.*, **255**, 341–350.

Srivastava, S.P., Kumar, K.U. & Kaufman, R.J. (1998) Phosphorylation of eukaryotic translation initiation factor 2 mediates apoptosis in response to activation of the double-stranded RNA-dependent protein kinase. *J. Biol. Chem.*, **273**, 2416–2423.

Uehara, T., Nakamura, T., Yao, D., Shi, Z.Q., Gu, Z., Ma, Y., Masliah, E., Nomura, Y. & Lipton, S.A. (2006) S-nitrosylated protein-disulphide isomerase links protein misfolding to neurodegeneration. *Nature*, **441**, 513–517.

Vrabec, J.P. & Levin, L.A. (2007) The neurobiology of cell death in glaucoma. *Eye*, **21**, S11–S14.

Wang, X., Sam-Wah, T.S. & Ng, Y.K. (2000) Nitric oxide, microglial activities and neuronal cell death in the lateral geniculate nucleus of glaucomatous rats. *Brain Res.*, **878**, 136–147.

Weber, A.J., Chen, H., Hubbard, W.C. & Kaufman, P.L. (2000) Experimental glaucoma and cell size, density, and number in the primate lateral geniculate nucleus. *Invest. Ophthalmol. Vis. Sci.*, **41**, 1370–1379.

Yücel, Y.H. & Gupta, N. (2008) Glaucoma of the brain: a disease model for the study of transsynaptic neural degeneration. *Prog. Brain Res.*, **173**, 465–478.

Yücel, Y.H., Zhang, Q., Gupta, N., Kaufman, P.L. & Weinreb, R.N. (2000) Loss of neurons in magnocellular and parvocellular layers of the lateral geniculate nucleus in glaucoma. *Arch. Ophthalmol.*, **118**, 378–384.

Yücel, Y.H., Zhang, Q., Weinreb, R.N., Kaufman, P.L. & Gupta, N. (2001) Atrophy of relay neurons in magno- and parvocellular layers in the lateral geniculate nucleus in experimental glaucoma. *Invest. Ophthalmol. Vis. Sci.*, **42**, 3216–3222.

Yücel, Y.H., Gupta, N., Zhang, Q., Mizisin, A.P., Kalichman, M.W. & Weinreb, R.N. (2006) Memantine protects neurons from shrinkage in the lateral geniculate nucleus in experimental glaucoma. *Arch. Ophthalmol.*, **124**, 217–225.

© 2011 The Authors. European Journal of Neuroscience © 2011 Federation of European Neuroscience Societies and Blackwell Publishing Ltd